Hydraulic Redistribution Decreases with Precipitation Magnitude and Frequency in a Dryland Ecosystem: A Data-Model Fusion Approach

Aneesh Kumar Chandel[1], Mitra Cattry[3], Yu Zhou[4], Hang Duong[2,5], Marcy Litvak[2], William Pockman[2] and Yiqi Luo[1]

[1]School of Integrative Plant Science, Cornell University, Ithaca, NY, USA

[2]Biology Department, University of New Mexico, Albuquerque, NM, USA

[3]Department of Earth and Environmental Engineering, Columbia University, USA

[4]Department of Environmental Systems Science, ETH Zurich, Switzerland

[5]Vietnam National University of Agriculture, Hanoi, Vietnam

Corresponding Authors: Aneesh Kumar Chandel (akc76@cornell.edu), Yiqi Luo (yl2735@cornell.edu)

Abstract

Hydraulic redistribution (HR), the movement of water via plant root systems that connect soil compartments with different water potential, should influence soil moisture dynamics particularly in dryland ecosystems, where water availability strongly constrains ecosystem function. Realistic representation of HR in ecosystem models is essential to improve the ability of these models to predict ecosystem function in dryland regions. In this study, we integrated HR into the Terrestrial ECOsystem model and employed a Bayesian Markov Chain Monte Carlo technique to optimize soil hydraulic parameters and root conductance using four years of soil moisture observations from a piñon-juniper woodland. We found that (i) integrating HR generally improved model prediction of soil moisture during dry periods, particularly in the top 30 cm of the soil profile, where more than 50% of root biomass exists; (ii) HR increased surface soil moisture by up to 60% during dry periods; (iii) HR decreased with increasing precipitation magnitude and frequency, however, the length of dry spells between rainfall events also influenced HR rates; and (iv) upward HR in the top 60 cm soil profile became more pronounced as dry conditions progressed, with rates ranging from 0.10 to 0.50 mm d^{-1}. These findings highlight that HR plays a critical role in sustaining soil moisture during extended dry periods and has a limited effect during precipitation events. Future research should investigate the effect of HR on other ecosystem processes, such as net ecosystem exchange of carbon and evapotranspiration under varying climatic conditions.

1. Introduction

Soil volumetric water content (VWC), defined as the amount of water stored in the unsaturated zone of the soil profile, is a fundamental state variable regulating ecosystem water and energy exchanges, particularly in dryland ecosystems (Seneviratne et al., 2010). Drylands cover over 40% of Earth's terrestrial surface and support more than 38% of the global population (Prăvălie, 2016), underscoring the importance of understanding soil moisture dynamics in these regions. While VWC provides a useful measure of soil water status, the movement and availability of this water are governed by soil water potential, particularly its matric component, which reflects the capillary and adsorptive forces binding water to soil particles (Hillel, 2003; Novick et al., 2022). In unsaturated soils, matric potential determines how tightly water is retained and how readily it can move toward plant roots. Because dryland ecosystem functioning is strongly constrained by precipitation variability (Beer et al., 2010; Ukkola et al., 2021), understanding how plants regulate water under fluctuating moisture conditions is essential for predicting ecosystem stability.

One key mechanism underlying this regulation is hydraulic redistribution (HR), the passive movement of water through plant roots, usually at night, from wet to dry regions of the plant rooting volume driven by differences in water potential. This passive process can favor plant survival during droughts by tapping into deep soil layers having relatively higher water potential and redistributing water to the shallow root zone (upward HR) (Nadezhdina et al., 2015; Prieto et al., 2012; Nicola and Ram, 2022). During wet seasons, HR can redistribute water from wet surface soil into deeper, drier soil (downward HR), supplementing the infiltration process in recharging deeper soil layers (Hultine et al., 2003; Scott et al., 2008; Fu et al., 2016; Bleby et al., 2010). Despite its potential role in regulating plant and ecosystem productivity, nutrient cycling

and soil microbial activity (Grünzweig et al., 2022; Sardans and Peñuelas, 2014), most current dynamic global vegetation models and Earth system model still lack an explicit representation of HR (Fu et al., 2016).

HR has been observed across diverse ecosystems and plant species (Neumann and Cardon, 2012; Nadezhdina et al., 2010; Yu et al., 2013; Priyadarshini et al., 2016). It is recognized as a structural driver of dryland plant communities, regulating ecosystem productivity, and enhancing resilience to climate extremes (Lee et al., 2018; Barron‐Gafford et al., 2021; Barron‐Gafford et al., 2017; Hafner et al., 2020). The dynamics of HR are influenced by various biotic (rooting architecture, plant capacitance, transpiration demand, senescence, and dormancy), abiotic factors (soil hydraulic characteristics, soil moisture status), and climatic conditions (precipitation) (Prieto et al., 2012; Katul and Siqueira, 2010; Wei et al., 2022). While several studies in arid and semi-arid ecosystems have reported upward HR during dry periods (Hao et al., 2013a; Lee et al., 2018; Scott et al., 2008; Yu et al., 2013) and downward HR following precipitation (Hultine et al., 2003), study on the fine-scale temporal variability of HR across multiple soil depths and multi-year timescales remains limited. Moreover, a quantitative understanding of how precipitation magnitude and frequency, key limiting factors in dryland ecosystems, influence HR rates is still lacking.

In this study, we explicitly test two hypotheses: (1) Direction of HR: Upward HR should be the dominant form of HR in dryland ecosystem. This is due to the recharge of deeper soil layers from precipitation which can retain moisture for longer periods, and during dry periods roots facilitate the movement of this retained water to the drier surface soils. (2) HR-precipitation relationship: Upward HR should decline following precipitation events, reaching its maximum rates during prolonged dry periods as drought creates steep water potential gradients between

89 deeper, moist soil layers and the drier surface layers, facilitating the upward redistribution of
90 water.

91 Meanwhile, soil moisture dynamics are governed by a complex interplay of forces that drive
92 water movement through the soil profile. The primary drivers include matric potential (capillary
93 and adsorptive forces binding water to soil particles), gravitational potential (driving downward
94 drainage), and HR (Caldwell et al., 1998). These forces collectively determine soil water
95 retention, redistribution, and plant water availability (Hillel, 2003). However, isolating their
96 individual contributions from field soil moisture observations is challenging, because these
97 processes operate simultaneously and are strongly influenced by soil properties, root activity, and
98 atmospheric conditions. Consequently, a data-model fusion approach, which integrates process-
99 based models with soil moisture observations, provides a robust framework to isolate and
100 quantify HR, offering a more mechanistic and quantitative understanding of soil-plant water
101 dynamics.

102 Several modeling studies have incorporated various HR schemes into process-based models
103 to improve understanding of hydrological and ecological processes (Ryel et al., 2002; Amenu
104 and Kumar, 2008; Wu et al., 2020; Fu et al., 2016; Zheng and Wang, 2007; Tang et al., 2015;
105 Lee et al., 2018; Quijano and Kumar, 2015). However, realistic representation and estimation of
106 parameters related to HR remains a challenge, as neither the magnitude of HR nor its associated
107 parameters can be directly observed in the soil (Ryel et al., 2002; Quijano and Kumar, 2015). As
108 a result, most models rely on default HR parameter values derived from Ryel et al. (2002). For
109 example, in a study by Fabian et al. (2010), the maximum soil-root radial conductance (C_{RT}), a
110 key parameter controlling HR, was assigned as the mean value between C_{RT} reported by Ryel et
111 al. (2002) for *Artemisia tridentata* and by Williams et al. (1996) for *Quercus-Acer* stand.

Similarly, Zheng and Wang (2007) and Yan and Dickinson (2014) prescribed a constant C_{RT} value based on Ryel et al. (2002). Alternatively, some studies estimated parameters during specific periods of time when upward or downward HR is assumed negligible, such as wet or dry season (Fu et al., 2018; Fu et al., 2016). These challenges in direct measurement, the reliance on assumed parameter values, and the parameterization of HR under the assumption of negligible redistribution constitute key gaps in our understanding of HR dynamics.

To address these gaps, we focused on piñon-juniper (PJ) woodlands, the most widespread semi-arid ecosystem in the US. PJ woodlands are spatially widespread, ecologically important, temporally dynamic, and structurally unique dryland ecosystem in the western US, spanning 10 US states and 40 million hectares across the American Southwest (Eastburn et al., 2024; Romme et al., 2009). Despite their importance, HR has not been previously studied in PJ woodlands. However, our continuous root sap flux measurements provided direct evidence of HR in both piñon and juniper roots, indicated by sustained negative root sap flux during nighttime at the study site (Fig. S1).

In this study, we used the process-based Terrestrial ECOsystem (TECO) model to (i) develop and implement a data assimilation approach to integrate HR into the TECO model; (ii) quantify and characterize the magnitude and dynamics of HR across multiple soil depths; and (iii) analyze the temporal patterns of HR and its relationship with precipitation magnitude and frequency. The TECO model is a well-established ecosystem model that integrates ecological processes to simulate carbon, water, and energy fluxes within terrestrial ecosystems (Weng and Luo, 2008). We employed data assimilation to constrain the TECO model including HR using four years of soil moisture data measured at multiple soil depths, encompassing both wet and dry periods.

2. Data and Methods

2.1 Study site and data

Our modeling study utilized data from a PJ woodland plot (Lat. 35.642, Long. -104.607, elevation 1925 m) located in New Mexico, USA, and previously described in Schwinning et al. (2020). The site is a private ranch covering an area of over 6800 hectares that was ungrazed from 2012 through the measurement period used for this study and is characterized by a semi-arid climate. Mean annual precipitation of the site is approximately 460 mm, with the majority falling between May and October, and a mean annual temperature of 10.5 °C. The soil texture at the site varies with depth, ranging from loam to clay loam. The vegetation consists of distinct tree clusters dominated by piñon pine (*Pinus edulis* (Englem.)) and juniper (*Juniperus monosperma* (Englem.) Sarg.) separated by open areas of bare soil and herbaceous cover.

VWC was continuously monitored using multi-sensor frequency domain capacitance probes (Decagon EC-5) installed at four depths (5, 15, 30 and 60 cm), in four soil pits under the tree canopies. All sensors were monitored every minute by a datalogger (model CR6, Campbell Scientific), and 15-minute averages were stored. For model parameterization, we used 15-min VWC records aggregated to daily means. Each sensor was calibrated in the lab before installation for both air and water frequency. Because soil temperature can affect both soil permittivity and the response of capacitance sensors, potentially confounding the small fluctuations in VWC caused by HR, temperature correction factors were applied to the measured VWC at each depth, using the nearest measured temperature, following the method described by Saito et al. (2009). Rather than excluding data below 0 °C, we used this temperature-correction approach to reduce the influence of temperature-driven artifacts on the soil moisture signal. This

strategy allows retention of continuous soil moisture records while accounting for the known sensitivity of capacitance sensors to temperature-dependent changes in dielectric permittivity.

2.2 Modeling framework

TECO is a process-based ecosystem model (Hou et al., 2021; Jiang et al., 2018; Weng and Luo, 2008), and has evolved from the TCS model (Luo and Reynolds, 1999). The model consists of major components: canopy photosynthesis, plant growth, soil water dynamics, and soil carbon transfers. The canopy photosynthesis and soil water dynamics submodels run at the hourly time step whereas the plant growth and soil carbon submodels run at the daily time step. The model is driven by seven environmental variables, including precipitation (mm), wind speed (m s^{-1}), solar radiation (W m^{-2}), air and soil temperature (C), relative humidity (%), and vapor pressure deficit (kPa). The detailed description of TECO model is available (Weng and Luo, 2008) and only a brief description of soil water dynamics is provided here.

The soil profile is divided into 10 layers with a total depth of 180 cm, with varying thickness: 5 cm for the first layer, 10, 15, and 30 cm for the second, third, and fourth layers respectively, and 20 cm for each of the fifth through tenth layers. VWC in each layer results from the mass balance between influx and efflux, with changes primarily attributed to vertical unsaturated flow, transpiration, precipitation, runoff, and drainage. Evaporation depletes water from the first two soil layers, while transpiration depletes water from all soil layers containing roots, allocated based on root fraction in each layer (Eq. 8). Given the predominantly arid conditions of the study site, runoff and drainage were found negligible. Thus, water movement between soil layers is simulated as follows:

$$\frac{dW_i}{dt} = \frac{dF_i}{dz} - E_i - T_i \quad (1)$$

where W_i is the water storage (cm) in layer i, t is time (h), F_i is net unsaturated flow of water into layer i (cm h^{-1}), z is vertical thickness, E_i and T_i are evaporation and transpiration water loss from layer i (cm h^{-1}).

The unsaturated soil water movement is simulated vertically according to modified form of Buckingham-Darcy's law (Campbell, 1985) (Eq. 2), with Brooks (1965) equation (Eq. 4) estimating hydraulic conductivity and soil water retention curve (SWRC) to simulate soil water potential (Ψ).

$$\frac{dF_i}{dz} = \mathrm{K}(\theta_i)\left(\frac{d\Psi_i}{dz} + 1\right) \quad (2)$$

where $K(\theta_i)$ is the unsaturated soil hydraulic conductivity (cm h^{-1}) for VWC θ (cm^3 cm^{-3}) in layer i, Ψ_i is soil water matric potential (MPa) in layer i, and z is the vertical thickness (cm) of the soil.

$$\mathrm{K}(\theta_i) = K_s \left[\frac{\theta_i - \theta_r}{\theta_s - \theta_r}\right]^{(2m+3)} \quad (3)$$

where, K_s is the soil saturated hydraulic conductivity (cm h^{-1}), m is the pore size distribution index, θ_s and θ_r are saturated and residual VWC (cm^3 cm^{-3})

$$\frac{\theta - \theta_r}{\theta_s - \theta_r} = \left(\frac{\Psi}{\Psi_b}\right)^{-1/m} \quad (4)$$

Ψ_b is the soil air entry water potential.

To quantify the direction and magnitude of HR, we integrated the HR model by Ryel et al. (2002) into equation 1 of TECO model (Eq. 5). This HR model empirically describes HR flux based on the soil water potential gradient between two soil layers (Eq. 6). HR was assumed to occur only at night, with its occurrence controlled by solar radiation instead of fixed day and night hours. Daytime starts as solar radiation exceeds 10 W m^{-2}, thereby inhibiting HR since the water potential gradient typically favors water movement from roots to canopy to meet

transpiration demand during the day. This pattern is evident in Fig. S1, where under low or zero solar radiation, root sap flux was found to be negative, indicating water movement away from the root zone which is an indicator of occurrence of HR at the study site. Using these assumptions, the net water movement into soil layer *i* from other soil layers *j* can be expressed as:

$$\frac{dW_i}{dt} = \frac{dF_i}{dz} - E_i - T_i + H_i \quad (5)$$

$$H_i = C_{RT} \sum_j (\Psi_j - \Psi_i) max\,(c_i, c_j) \frac{R_i R_j}{1 - R_x} D_{tran} \quad (6)$$

$$c_i = \frac{1}{1 + \left(\frac{\Psi_i}{\Psi_{50}}\right)^b} \quad (7)$$

$$R_{d,i} = \frac{R_0}{1 + \left(\frac{d_i}{d_{50}}\right)^a} \quad (8)$$

where in *Eq 6,* H_i is the net water redistributed by roots into layer *i* (cm h^{-1}) from other soil layers *j*, C_{RT} is the maximum radial soil-root conductance of the entire active root system for water (cm MPa^{-1} h^{-1}), Ψ is soil matric potential (MPa), c_i is a factor reducing soil-root conductance based on Ψ_i, R_i is the fraction of active roots in layer *i*, R_0 is the average vertically summed root dry mass from the bottom to the root zone to the soil surface, and D_{tran} is a factor reducing water movement among layers by roots while plant is transpiring and is assumed to be 1 during the night when transpiration is minimal and 0 during day. $R_x = R_i$ when $\theta_i > \theta_j$ or $R_x = R_j$ when $\theta_j > \theta_i$. In *Eq 7*, Ψ_{50} is the soil water potential (MPa) where conductance is reduced by 50% and *b* is an empirical constant. In *Eq 8*, $R_{d,i}$ is cumulative fraction of roots above soil depth d_i (cm) for the i^{th} layer, and d_{50} is the soil depth (cm) at the median of the root distribution and *a* is the shape parameter (Table 1). The Brooks (1965) model for SWRC was utilized to simulate soil water potential (Ψ), facilitating the development of soil water potential gradients necessary

for HR by tree roots (Eq. 4). Due to lack of site-specific parameters, the default values of b and Ψ_{50} were used as 3.22 and -1 MPa, respectively (Ryel et al., 2002).

2.3 Data assimilation for parameters estimation

We used Bayesian probabilistic inversion to calibrate parameters associated with soil hydraulics, where posterior probability density functions of parameters are obtained from prior knowledge about the parameters and the error between model and observations. According to Mosegaard and Sambridge (2002), Bayesian inversion can be summarized by the following equation:

$$p(c|Z) \propto p(Z|c)\, p(c) \tag{9}$$

where $p(c|Z)$ is posterior probability density function of model parameters c; $p(Z|c)$ is a likelihood function of parameters c; $p(c)$ is prior probability density function of parameters c. We assumed that the prediction errors were normally distributed and uncorrelated, hence, the likelihood function, $p(Z|c)$, was calculated as follows:

$$p(Z|c) \propto exp\left\{-\sum_{i=1}^{k} \frac{(Z_i - X_i)^2}{2\sigma_i^2}\right\} \tag{10}$$

where Z_i is observed VWC at i^{th} soil layer, X_i is VWC simulated by TECO at a corresponding soil depth; σ_i^2 is the variance of a measurement at a soil layer; k is the total number of soil layers.

To generate the posterior distributions, we first specified the priors of the parameters to be uniformly distributed over the intervals specified in Table 1. We put constraints on parameters based on literature. The initial set of parameters was randomly selected within the prior parameter ranges. Once we specified parameter ranges, we used the Metropolis-Hastings (M-H) algorithm (Hastings, 1970; Metropolis et al., 1953), a Markov chain Monte Carlo method, to

sample from the posterior parameter distribution. To generate a parameter set, we ran M-H algorithm in two steps: proposing step and moving step. In the proposing step, a new parameter set c^{new} was generated from a previously accepted parameter set c^{k-1} through a proposal distribution $(c^{new}|c^{k-1})$:

$$c^{new} = c^{k-1} + r \times \frac{c^{max} - c^{min}}{D} \quad (11)$$

The value of $P(c^{k-1}|c^{new})$ was then compared with a random number U from 0 to 1. Parameter set c^{new} was accepted if $P(c^{k-1}|c^{new}) \geq U$, otherwise c^{k} was set to c^{k-1}. In the moving step, a probability of acceptance $P(c^{k-1}|c^{new})$ was calculated as in the following (Marshall et al., 2004):

$$P(c^{k-1}|c^{new}) = min\left\{1, \frac{p(Z|c^{new})p(c^{new})}{p(Z|c^{k-1})p(c^{k-1})}\right\} \quad (12)$$

The M-H algorithm was repeated for 50,000 simulations, and then all accepted parameters values were used to generate the probability distribution functions (Xu et al., 2006).

To evaluate the impact of HR on soil moisture dynamics in a PJ woodland, we conducted two multi-year simulations using two configurations of the TECO model: TECO+HR (with HR) and default TECO (HR turned off). To distinguish the influence of HR from soil hydraulic properties, we adopted a data assimilation approach focused on calibrating only the TECO+HR model. Soil moisture observations were available at 5, 15, 30 and 60 cm depths, and data assimilation was therefore applied only to these four soil layers over a four-year period, and data-model comparisons are presented exclusively for these depths. The parameters values deeper than 60 cm were not calibrated and were empirically defined from literature values. This modeling strategy is consistent with other data assimilation studies, in which model calibration is restricted to soil layers with available observations (Fu et al., 2016; Zhang et al., 2016). In total,

21 parameters were optimized including 20 soil hydraulic parameters (θ_s, θ_r, K_s, m, and Ψ_b for each of the four soil depths) across four soil layers and one HR-related parameter (C_{RT}). The prior range of soil hydraulic parameters were informed by established relationships between soil texture and hydraulic properties (Rawls et al., 1982; Clapp and Hornberger, 1978). The prior range for C_{RT} was based on values reported in Fu et al. (2016). Within this range, we optimized depth-specific soil hydraulic parameters to achieve a close match between modeled and observed soil moisture (Table 1).

After calibrating the TECO+HR model, we deactivated the HR process and ran simulations with the same optimized parameters to generate the default TECO scenario. Before each model simulation, we performed a 200-year spin-up separately for both model configuration (TECO+HR with HR active and default TECO with HR disabled) to ensure that each model reached stable carbon stocks as initial conditions.

The motivation to calibrate only TECO+HR model, rather than the default TECO is to avoid parameter compensation for unresolved processes (Luo and Schuur, 2020), in which the absence of HR could lead to unrealist adjustments of soil hydraulic parameters to indirectly capture its effects. This approach allowed us to ensure that differences in soil moisture dynamics between TECO+HR and default TECO simulations were attributable solely to the presence or absence of HR.

Furthermore, to evaluate the influence of cumulative precipitation and soil moisture memory on HR, we calculated the Antecedent Precipitation Index (API) for the study period (2018–2021) following Kohler and Linsley (1951). API acts as a proxy for soil moisture status by accounting

for the decaying effect of past rainfall events. The daily API (API_t) was calculated using the recursive decay function:

$$API_t = P_t + (k*API_{t-1}) \quad (13)$$

where P_t is the precipitation on day t (mm), API_{t-1} is the index value of the preceding day, and k is a decay constant representing the recession of soil moisture due to evapotranspiration and drainage. We used a decay constant of $k = 0.90$, which falls within the commonly applied range for antecedent precipitation indices and is consistent with optimization analyses indicating optimal decay constants near 0.90 (Li et al., 2021). This metric enables differentiation between short dry intervals following wet conditions and extended dry spells with limited antecedent moisture.

2.4 Statistical analysis

Model performance was assessed by comparing simulated outputs with observed data during full simulation periods (2018- 2021), dry, and wet periods, defined as days without and with rainfall events, respectively. During the study period, wet days accounted for 22% of all days, whereas dry days comprised the remaining 78%. Model performance was evaluated using two statistical metrics: root mean square error (RMSE) and absolute mean error (MAE). RMSE is widely used to quantify model accuracy, but its squared-error formulation overemphasizes the effects of large deviations (Willmott and Matsuura, 2005). Therefore, MAE was also calculated as a measure of the average magnitude of deviation from observed values (Alfieri et al., 2017). Both metrics were calculated as follows:

$$RMSE = \sqrt{\frac{1}{n}\sum_{i=1}^{n}(m_i - o_i)^2} \quad (14)$$

$$MAE = \frac{1}{n}\sum_{i=1}^{n}|m_i - o_i|^2 \quad (15)$$

Where: o_i represents observed values, m_i represents modeled values, and n represents the number of data points.

Table 1: Parameters constrained using data assimilation in the TECO model from soil moisture data from 2018 to 2021.

Parameters	Symbols	Constrained values	Range	Units	References
Saturated water content	θ_s	0.34/0.38/0.36/0.33	[0.3, 0.4]	$cm^3\ cm^{-3}$	Calibrated
Residual water content	θ_r	0.05/0.07/0.06/0.03	[0, 0.08]	$cm^3\ cm^{-3}$	Calibrated
Saturated hydraulic conductivity	K_s	0.14/0.29/0.30/0.70	[0.1, 2]	$cm\ h^{-1}$	Calibrated
Pore size distribution	m	0.89/0.66/0.88/0.84	[0, 1]	-	Calibrated
Air entry water potential	Ψ_b	96/60/50/40	[0, 100]	cm	Calibrated
Maximum radial soil-root conductance	C_{RT}	0.022	[0, 1]	$cm\ MPa^{-1}\ h^{-1}$	Calibrated
Soil Ψ where root conductivity reduced by 50%	Ψ_{50}	-1.0	-	MPa	(Ryel et al., 2002)
Empirical constant	b	3.22	-	-	(Ryel et al., 2002)
Average vertically summed root dry mass	R_0	0.90	-	$kg\ m^{-2}$	(Schwinning et al., 2020)
Soil depth at the median of the root distribution	D_{50}	25	-	cm	(Schwinning et al., 2020)
Root distribution shape parameter	a	2.2	-	-	(Schwinning et al., 2020)

Four values represent parameters in the four modeled VWC at depths of 5, 15, 30, and 60 cm, respectively.

3. Results

3.1 Parameter estimation via data assimilation and water mass balance

The data assimilation approach, using VWC data to constrain the model, yielded well-constrained soil hydraulic parameters (Table 1; Fig. S2 and S3). The resulting posterior probability density functions, characterized by sharp peaks, narrow spread, and consistency across soil depth support the reliability and accuracy of these calibrated parameter values. Additionally, soil water mass balance of soil profile was conserved before and after incorporating the HR process into the TECO model (Fig. S4). The key components of the water budget: precipitation, evapotranspiration, and changes in soil water content remained balanced, ensuring that the model accounted for all water fluxes. Furthermore, the sum of HR across all soil layers (10 layers) was consistently equal to zero, further ensuring that no water was artificially introduced or lost from the system.

3.2 Observed and simulated soil moisture

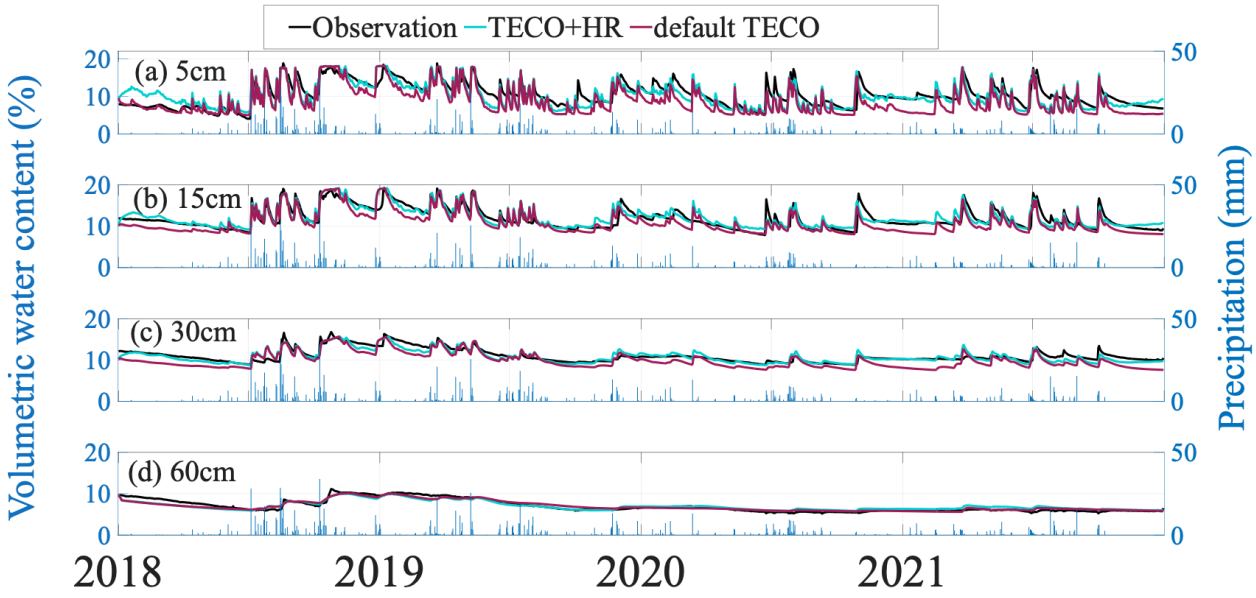

Figure 1a-d: Observed and simulated soil volumetric water content (from January 2018 to December 2021) at soil depths of 5 cm (a), 15 cm (b), 30 cm (c), and 60 cm (d). Black lines indicate observations, cyan lines indicate TECO+HR, and magenta lines indicate default TECO. Vertical blue bars indicate daily precipitation (right axis).

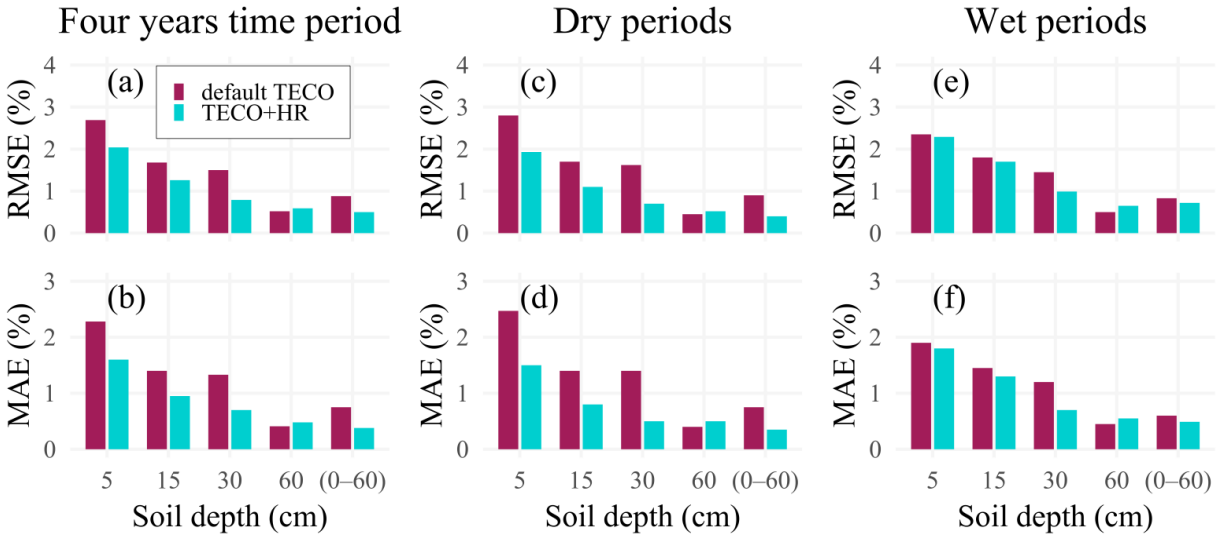

Figure 2: Model performance for soil moisture across different depths (5, 15, 30, and 60 cm, and 0-60 cm integrated soil profile), considering temporal variations in soil moisture conditions. Root Mean Square Error (RMSE, %) and Mean Absolute Error (MAE, %) are presented for the complete time series (a, b), dry periods (c, d), and wet periods (e, f). Lower values of RMSE and MAE indicate better model performance.

346 The data assimilation-constrained models generally captured both the magnitude and
347 dynamics of observational data, reproducing seasonal variations in soil moisture across four soil
348 depths. Minor mismatches at the topsoil (5 cm) likely reflect the complexity of near-surface
349 processes that are not fully represented in simplified models and potential sensor lag due to
350 imperfect soil contact, as similar discrepancies are not observed at deeper layers. In addition,
351 following prolonged dry periods, initial rainfall can be largely offset by evaporation, resulting in
352 muted surface soil moisture responses (Miele et al., 2023; Cattry et al., 2025; Asadollahi et al.,
353 2022). While TECO+HR simulation showed an improvement in the overall model performance,
354 the impact of HR was mostly pronounced during dry periods (Figs. 1 and 2). We further
355 examined diurnal soil moisture fluctuations (Fig. S5) and found that TECO+HR closely tracked
356 the observed diurnal cycles, whereas the default TECO failed to capture this pattern, suggesting
357 that the observed diurnal variability was likely driven by HR. Additionally, we compared min-
358 max normalized soil matric potential at 15, 30, and 60 cm with simulations derived from Eq. (4)
359 (Fig. S6). Both models reproduced the general trends of the observations, suggesting that the
360 simulated soil water potential gradients were consistent with measurement.

361 Moreover, during periods of limited precipitation, the TECO+HR (blue lines) consistently
362 maintained higher soil moisture compared to default TECO (red lines), aligning closer to
363 observation particularly in the topsoil layers (Fig. 1a-c). Following precipitation events, the
364 default TECO and TECO+HR simulations converged, suggesting the minimal influence of HR
365 under wet conditions at the study site. However, as surface soil moisture decreased following
366 precipitation, the two simulations diverged again, with TECO+HR maintaining higher moisture
367 levels in the topsoil layers, highlighting the role of HR in maintaining soil moisture during
368 prolonged drought.

The incorporation of HR into TECO resulted in reductions in model errors. During dry periods, the RMSE decreased by 25, 43, and 52% at 5, 15, and 30 cm soil depths, respectively. However, limited improvement was observed at 60 cm soil depth. Correspondingly, the MAE was reduced by 30, 53, and 60% at 5, 15, and 30 cm, respectively. Over the entire study period, RMSE decreased by 24, 25, and 47% at 5, 15, and 30 cm, with MAE reductions were 29, 34, and 55% at the same depths (Fig. 2a-d). Overall soil profile performance improved as well, with RMSE and MAE reductions over 40% for both the four-year simulation and dry periods. These improvements during dry periods are especially important, as roots are most vulnerable to drought. By mitigating soil water deficits in surface layers, HR could reduce the risk of hydraulic failure, thereby supporting plant species survival and it could enable better prediction of ecosystem responses to water stress, such as carbon uptake (Domec et al., 2010), and evapotranspiration (Zhu et al., 2017). In contrast, during wet periods, HR had minimal influence on soil moisture (Fig. 2e, f).

3.3 Effect of HR on soil moisture

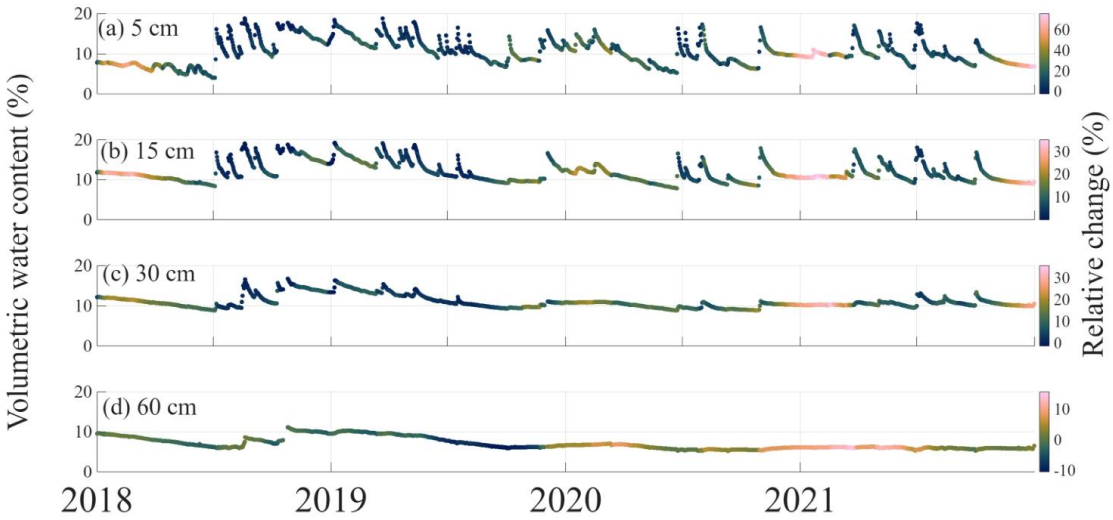

Figure 3: Relative change in modeled volumetric water content (VWC, %) across four soil depths (5, 15, 30, and 60 cm). The color gradient represents the relative change (%) in modeled VWC, calculated as (HR−No HR)/No HR×100, with HR and No HR indicating simulations with and without hydraulic redistribution, respectively. The relative change is overlaid on observed VWC.

The direct impact of HR on hydrological processes should be evident in the soil profile water content. We tested this by comparing VWC model simulations in TECO with and without HR processes, to observed VWC time series at four depths (Fig. 3). We found that cumulative effects of HR on soil moisture vary with depth, primarily due to the non-uniform root biomass distribution throughout the soil profile (Fig. S8). The most pronounced effects of HR were observed in the topsoil layers (5, 15, and 30 cm), where average daily water content increased by up to 60% compared to simulation without HR. This increase was driven by upward HR, especially during dry-down periods (Fig. 4b).

3.4 HR simulations

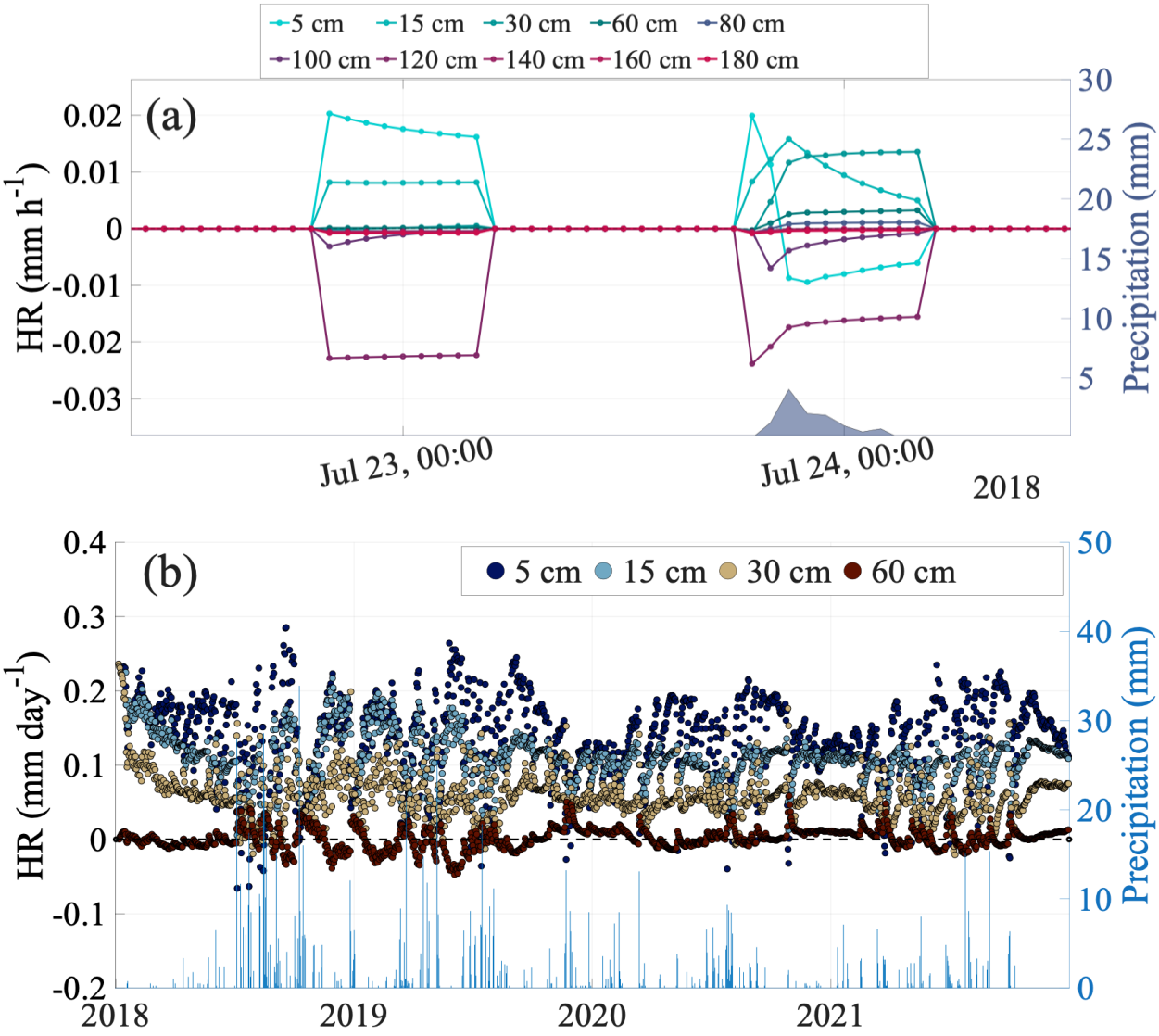

Figure 4: Temporal dynamics of hydraulic redistribution (HR). (a) diurnal pattern of modeled HR across soil depths from July 22-24, 2018. The graph illustrates HR patterns during a dry period followed by a precipitation event (right y-axis). Colored lines represent different soil depths. (b) long-term daily HR trends and precipitation from January 2018 to December 2021. The blue vertical bars represent precipitation (right y-axis).

Model simulation revealed distinct patterns of HR dynamics across soil depths and temporal scales. Fig. 4 illustrates these patterns over two timescales: a short-term, diurnal pattern (Fig. 4a), and a long-term perspective from 2018 to 2021 (Fig. 4b). HR is a process with both a source and

404 a sink for water movement. In Fig. 4, positive HR suggests that a soil layer is gaining water
405 (sink), whereas negative HR values suggest that the layer is losing water (source).

406 The short-term modeling analysis highlights diurnal pattern of HR during dry conditions and
407 a precipitation event (Fig. 4a). For instance, on July 23, 2018, during a dry period, upward HR
408 occurred, moving water from deeper (> 100 cm) to shallower (0-30 cm) soil layers. However,
409 following a precipitation event on July 24, 2018 (12 mm), this pattern shifted. The top 5 and 15
410 cm layers showed negative HR and a decrease in the upward HR rate, respectively, acting as a
411 water source for deeper layers. At the same time, deeper soil layers showed a decline in negative
412 HR rates, suggesting signs of receiving water likely from the topsoil layers. The sum of HR
413 across all soil layers remained zero, confirming that HR redistributed water rather than adding to
414 the system. Consequently, downward HR from the topsoil supplemented infiltration, enhancing
415 water movement into deeper soil layers, reflected by a decrease in the negative HR rates at
416 depths and an increase in the positive HR rate at 30 cm (Fig. 4a).

417 While our model simulates HR across 10 soil layers, we present long-term results for only
418 the top four soil layers (5, 15, 30, and 60 cm) to enable direct comparison with the available
419 observed soil moisture data. A clear seasonal pattern emerged, with HR generally intensifying
420 during dry periods (Fig. 4b).

421 Our model showed that upward HR was predominantly occurring in up to top 30 cm of soil
422 profile, with values ranging from -0.066 to 0.29 mm d^{-1} in each soil layer and an average of 0.30
423 mm d^{-1} across the top 30 throughout the study period. Downward HR, while less pronounced,
424 moved water only from the 5 cm soil layer during monsoon seasons and large precipitation
425 events (e.g., July 2018, 2019, 2020, and 2021; Fig. 4b). In contrast, 60 cm soil layer typically
426 exhibits a negative HR during dry periods, acting as a water source for upper layers, and positive

HR during wet periods, suggesting occasional water input from surface layers ranging from -0.096 to 0.059 mm d^{-1} (mean 0.0015 mm d^{-1}). Moreover, integrated soil profile (top 60 cm of soil profile), showed that upward HR was the dominant form of HR throughout the year, ranging from 0.10 to 0.53 mm d^{-1} with a mean value 0.31 mm d^{-1} (Fig. S7).

3.5 Precipitation influences on HR

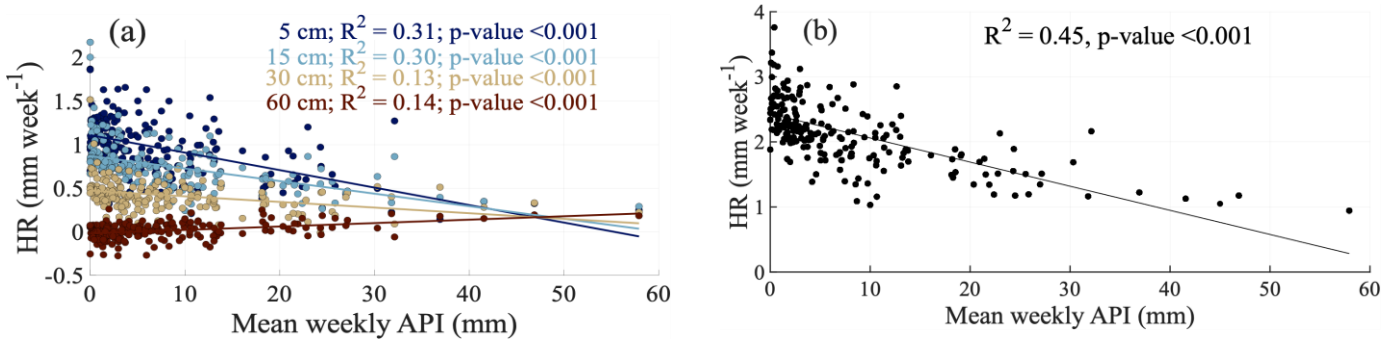

Figure 5: Relationships between hydraulic redistribution (HR) and Antecedent Precipitation Index (API). (a) Weekly HR rates versus mean weekly API at different soil depths (5, 15, 30, and 60 cm). For each soil depth, the trend lines, R², and corresponding p-values are shown. (b) Depth-integrated weekly HR across 0–60 cm soil profile versus mean weekly API, with trend line, R², and p-value.

The model results showed a significant linear relationship between weekly HR and mean weekly API (mm) (Fig. 5a-b). In the topsoil layers (5 cm and 15 cm), HR exhibited negative relationships with API (R^2 = 0.31 and 0.30 respectively, both p-values < 0.001), indicating that HR activity decreased as antecedent moisture conditions became wetter. In contrast, positive correlation was observed at 30 and 60 cm depths (R^2 = 0.13 and 0.14 respectively, both p-values < 0.001), suggesting downward redistribution under wetter antecedent conditions.

Additionally, when HR was integrated across the soil profile (0-60 cm), a significant negative relationship with mean weekly API was observed (R^2 = 0.45, p-values < 0.001, Fig. 5b). This suggests that overall HR activity was greatest under drier antecedent conditions and

441 declined as cumulative moisture availability increased, highlighting the stronger role of HR in
442 regulating soil water dynamics during prolonged dry periods.

443 Despite these clear trends, variability in HR was observed across the full range of mean
444 weekly API values (Fig. 5a-b). This
445 variability could be attributed to the rainfall
446 frequency, event size, and the duration of
447 dry periods between rainfall events (Fig.
448 6), factors that are implicitly captured by
449 API. Figure 6 provides a more detailed
450 view of these controls by relating HR
451 directly to dry spell length and rainfall
452 frequency, suggesting that HR may
453 increase not only with reduced

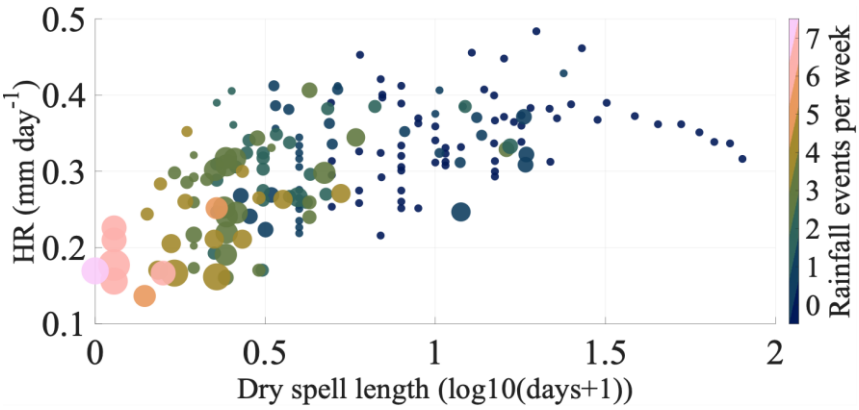

Figure 6: Relationship between weekly mean hydraulic redistribution (mm d^{-1}), dry spell length between two rainfall events (log_{10}(days+1)). The color scale indicates the number of rainfall events per week, while marker size represents the weekly precipitation amount (mm $week^{-1}$). Dry spell length denotes the number of rainless days between two consecutive precipitation events. The x-axis shows dry spell length transformed as log_{10}(days + 1) to allow inclusion of zero-length dry spells.

454 precipitation frequency but also as the interval between consecutive rainfall events lengths. HR.
455 HR was lowest under conditions of high rainfall frequency and shorter dry spells, progressively
456 increasing to its peak in the absence of rainfall. However, as the drought period extended beyond
457 30 days, HR declined, suggesting potential limitation on availability of deeper water to sustain
458 HR. This variability is further illustrated through three scenarios (Fig. S7): 1) Following a
459 rainfall event (28 mm on July 5, 2018), HR in the top 60 cm of soil profile was minimal at 0.13
460 mm d^{-1}, indicating limited driving force for water redistribution when soil moisture was
461 abundant. 2) During a transition period between rainfall events (July 5-10, 2018), HR gradually
462 increased but remained moderate, ranging from 0.13 to 0.20 mm d^{-1}, suggesting a progressive
463 activation of the redistribution process as soil began to dry. 3) During a prolonged dry period

(November 23-30, 2018), HR peaked at 0.20-0.52 mm d^{-1}, demonstrating enhanced redistribution activity in response to the development of soil moisture gradients.

4. Discussion

4.1 Patterns of hydraulic redistribution

Our findings support the hypothesis that upward HR is the dominant form of HR in dryland ecosystems due to limited precipitation amount and sporadic rainfall events (Fig. S7). This prevalence of upward water movement is characteristic of semi-arid regions, where deep-rooted plants often redistribute water from moist deeper layers to drier surface soils during periods of water stress (Caldwell et al., 1998; Ryel et al., 2002). Notably, the most pronounced HR occurred in the topsoil layer (5, 15, and 30 cm), (Fig. 4b), which can be attributed to vertical root distribution, with over 50% of root biomass concentrated in the top 30 cm (D_{50} = *25 cm*) of the soil profile (Fig. S8). Similar relationships between root distribution and HR intensity have been reported in previous studies, where deeper root systems extend redistribution to deeper soil layers, whereas shallow root systems amplify HR effects in surface soil due to higher root density and activity (Hao et al., 2013b).

The magnitude of HR simulated in this study (0.10-0.53 mm d^{-1} for top 60 cm soil) falls within the range reported in previous studies. Estimated HR rates for the topsoil were comparable to values synthesized in the global review by Neumann and Cardon (2012), which reported HR magnitudes ranging from 0.04 to 3.2 mm d^{-1} across ecosystem. However, our estimates are slightly higher than the upper range reported by Yang et al. (2022) for desert or sparsely vegetated ecosystems (0.014-0.475 mm d^{-1}). These differences likely reflect variations in vegetation structure, rooting depth, soil texture, and water availability among ecosystems.

4.2 Effects of precipitation variability on HR

Our findings support the hypothesis that the precipitation pattern significantly influences the magnitude and variability of HR (Figs. 4a-b, and S7). The rate of HR in the topsoil profile (<60 cm) exhibited a consistent response to precipitation events, characterized by sharp declines following large rainfall, and a gradual recovery to pre-rain levels during subsequent dry periods. Similar responses have been reported in previous study, where precipitation temporarily suppresses HR by reducing water potential gradients between shallow and deeper soil layers (Hao et al., 2013b). However, as water redistributes through the soil profile, new hydraulic gradients re-establish, leading to enhanced HR activity. In this phase, roots actively redistribute water from newly moistened deep layers to drier shallow layers (Yu and D'odorico, 2014; Ryel et al., 2002).

Our model predicted that HR rates were generally higher during rainless periods compared to rainfall periods within a given year. For instance, during the prolonged dry period in 2020 (driest year), HR rates remained consistently high, 0.17-0.40 mm d^{-1}, with minimal fluctuations. The consistent high HR rates, likely arises from more pronounced soil water potential gradients derived from sustained plant water demand and surface evaporation in the absence of frequent precipitation (Fu et al., 2016; Meinzer et al., 2004).

Seasonal patterns include higher HR rates (0.12-0.53 mm d^{-1}) during the drier periods (typically from November to May) and lower rates (0.10-0.30 mm d^{-1}) during the monsoon season (usually from June to October) (Fig. S7). This seasonality underscores the influence of both precipitation patterns and potential evapotranspiration on HR dynamics, highlighting that HR is likely more pronounced during drier seasons when soil moisture gradients are likely to be

more substantial due to reduced precipitation and potentially higher evaporative demand (Scott et al., 2008; Fu et al., 2016; Yu and D'odorico, 2014).

4.3 Limitation and future perspectives

While our modeling study provides valuable insights into HR dynamics in PJ woodlands, several limitations should be noted. (1) The model does not account for interannual changes in vegetation cover or species composition. Variations in plant functional types and leaf area index may influence soil moisture and HR, and incorporating these dynamics could improve long-term simulations. (2) Our analysis focused on the dominant tree species at study site; however, other plant species may also benefit from water redistributed by these trees, potentially influencing ecosystem water dynamics. (3) We did not include stem water refilling or nighttime transpiration reported by Howard et al. (2009) and Neumann et al. (2014), which may influence the magnitude of HR. (4) Finally, future studies should address these limitations and further investigate the role of HR in regulating ecosystem functions, such as carbon exchange and evapotranspiration.

5. Conclusions

This study demonstrates the role of hydraulic redistribution (HR) in soil water dynamics in piñon-juniper woodlands. By integrating HR processes and observations into the Terrestrial Ecosystem Model (TECO) via data assimilation, we successfully constrained model soil hydraulics parameters and improved simulations of soil water content across multiple depths, particularly in shallow soil layers (0–30 cm) and during dry periods. Our model results indicate that HR rates vary in response to the duration of dry spells between rainfall events. Generally, HR rates tend to increase as soil becomes drier and decreases with increasing precipitation

magnitude and frequency. Across the wet to dry transition, HR rates exhibit a range of 0.10 to 0.50 mm d^{-1}. Consequently, HR increased soil moisture in topsoil layers by up to 60% during dry periods, with upward HR emerging as the dominant flux, especially in the top 30 cm. These findings underscore the potential influence of HR during dry periods and highlight its role in sustaining soil water availability for vegetation. Future research should explore how HR-mediated water redistribution affects ecosystem functions including carbon exchange, and evapotranspiration.

6. Acknowledgments

This research is supported by US Department of Energy's Office of Biological and Environmental Research, Environmental System Science (ESS) Program (DE-SC0023514 to WTP, MEL and YL) and the modeling effort used data collected with funding from the US National Science Foundation (IOS 1557176 to MEL, WTP, and Susan Schwinning). Additional support from US NSF grants (DEB 2242034, DEB 2406930, and DEB 2425290), the US Department of Energy's Terrestrial Ecosystem Sciences Grant DE-SC0023514, subcontract CW55561 from Oak Ridge National Laboratory to Cornell University, and the "NYS Connects: Climate Smart Farms & Forestry" project, funded by the USDA, the New York State Department of Environmental Conservation, and the New York State Department of Agriculture and Markets. This research is also part of AI-CLIMATE: "AI Institute for Climate-Land Interactions, Mitigation, Adaptation, Tradeoffs and Economy", funded by the USDA National Institute of Food and Agriculture (NIFA), the NSF National AI Research Institutes Competitive Award (No. 2023-67021-39829) and Swiss National Foundation, Award#P500PN_206603 for their financial support of this collaboration.

7. Competing interests

The authors declare no competing interests.

8. Author contributions

AKC: Conceptualization, Methodology, Data curation, Formal analysis, Writing - original draft. **YZ:** Conceptualization, Writing - review & editing. **MC:** Writing - review & editing. **HD:** Writing - review & editing, Data curation. **ML:** Conceptualization, Data curation, Supervision, Writing - review & editing, Funding acquisition, Project administration. **WP:** Conceptualization, Data curation, Supervision, Funding acquisition, Writing - review & editing. **YL:** Conceptualization, Supervision, Project administration, Funding acquisition, Writing - review & editing.

9. Code and data availability

The Terrestrial ECOsystem (TECO) model code, along with the input data and model outputs used in this study, are archived on Zenodo at https://doi.org/10.5281/zenodo.18868950.

10. Supporting Information

Supporting information accompanying this manuscript is available in the supplement. The file includes supplementary figures referenced in the main text.

References

Alfieri, J. G., Anderson, M. C., Kustas, W. P., and Cammalleri, C.: Effect of the revisit interval and temporal upscaling methods on the accuracy of remotely sensed evapotranspiration estimates, Hydrology and Earth System Sciences, 21, 83-98, 10.5194/hess-21-83-2017, 2017.

Amenu, G. G. and Kumar, P.: A model for hydraulic redistribution incorporating coupled soil-root moisture transport, Hydrology and Earth System Sciences, 12, 55-74, 10.5194/hess-12-55-2008, 2008.

Asadollahi, M., Nehemy, M. F., McDonnell, J. J., Rinaldo, A., and Benettin, P.: Toward a closure of catchment mass balance: Insight on the missing link from a vegetated lysimeter, Water Resources Research, 58, e2021WR030698, 2022.

Barron‐Gafford, G. A., Knowles, J. F., Sanchez‐Cañete, E. P., Minor, R. L., Lee, E., Sutter, L., Tran, N., Murphy, P., Hamerlynck, E. P., and Kumar, P.: Hydraulic redistribution buffers climate variability and regulates grass‐tree interactions in a semiarid riparian savanna, Ecohydrology, 14, e2271, 2021.

Barron‐Gafford, G. A., Sanchez‐Cañete, E. P., Minor, R. L., Hendryx, S. M., Lee, E., Sutter, L. F., Tran, N., Parra, E., Colella, T., and Murphy, P. C.: Impacts of hydraulic redistribution on grass–tree competition vs facilitation in a semi‐arid savanna, New Phytologist, 215, 1451-1461, 10.1111/nph.14693, 2017.

Beer, C., Reichstein, M., Tomelleri, E., Ciais, P., Jung, M., Carvalhais, N., Rödenbeck, C., Arain, M. A., Baldocchi, D., and Bonan, G. B.: Terrestrial gross carbon dioxide uptake: global distribution and covariation with climate, Science, 329, 834-838, 2010.

Bleby, T. M., Mcelrone, A. J., and Jackson, R. B.: Water uptake and hydraulic redistribution across large woody root systems to 20 m depth, Plant, cell & environment, 33, 2132-2148, 2010.

Brooks, R. H.: Hydraulic properties of porous media, Colorado State University1965.

Caldwell, M. M., Dawson, T. E., and Richards, J. H.: Hydraulic lift: consequences of water efflux from the roots of plants, Oecologia, 113, 151-161, 10.1007/s004420050363, 1998.

Campbell, G. S.: Soil physics with BASIC: transport models for soil-plant systems, Elsevier1985.

Cattry, M., Miele, F., Wang, S., Frutschi, M., and Rinaldo, A.: Evaluating nitrate removal and travel times in a bare deciduous forest soil through a column tracer experiment, Catena, 258, 109204, 2025.

Clapp, R. B. and Hornberger, G. M.: Empirical equations for some soil hydraulic properties, Water resources research, 14, 601-604, 1978.

Domec, J. C., King, J. S., Noormets, A., Treasure, E., Gavazzi, M. J., Sun, G., and McNulty, S. G.: Hydraulic redistribution of soil water by roots affects whole-stand evapotranspiration and net ecosystem carbon exchange, New Phytol, 187, 171-183, 10.1111/j.1469-8137.2010.03245.x, 2010.

Eastburn, J. F., Campbell, M. J., Dennison, P. E., Anderegg, W. R., Barrett, K. J., Fekety, P. A., Flake, S. W., Huffman, D. W., Kannenberg, S. A., and Kerr, K. L.: Ecological and climatic transferability of airborne lidar-driven aboveground biomass models in Piñon-Juniper woodlands, GIScience & Remote Sensing, 61, 2363577, 2024.

Fabian, G. S., Sandra, J. B., William, A. H., Frederick, C. M., and Guillermo, G.: Hydraulic lift in a Neotropical savanna: Experimental manipulation and model simulations, Agricultural and Forest Meteorology, 150, 629-639, 10.1016/j.agrformet.2010.02.001, 2010.

Fu, C. S., Wang, G. L., Goulden, M. L., Scott, R. L., Bible, K., and Cardon, Z. G.: Combined measurement and modeling of the hydrological impact of hydraulic redistribution using CLM4.5 at eight AmeriFlux sites, Hydrology and Earth System Sciences, 20, 2001-2018, 10.5194/hess-20-2001-2016, 2016.

Fu, C. S., Wang, G. L., Bible, K., Goulden, M. L., Saleska, S. R., Scott, R. L., and Cardon, Z. G.: Hydraulic redistribution affects modeled carbon cycling via soil microbial activity and suppressed fire, Global Change Biology, 24, 3472-3485, 10.1111/gcb.14164, 2018.

Grünzweig, J. M., De Boeck, H. J., Rey, A., Santos, M. J., Adam, O., Bahn, M., Belnap, J., Deckmyn, G., Dekker, S. C., and Flores, O.: Dryland mechanisms could widely control

ecosystem functioning in a drier and warmer world, Nature ecology & evolution, 6, 1064-1076, 2022.
Hafner, B. D., Hesse, B. D., Bauerle, T. L., and Grams, T. E.: Water potential gradient, root conduit size and root xylem hydraulic conductivity determine the extent of hydraulic redistribution in temperate trees, Functional Ecology, 34, 561-574, 2020.
Hao, X. M., Chen, Y. N., Guo, B., and Ma, J. X.: Hydraulic redistribution of soil water in Populus euphratica Oliv. in a central Asian desert riparian forest, Ecohydrology, 6, 974-983, 10.1002/eco.1338, 2013a.
Hao, X. M., Li, W. H., Guo, B., and Ma, J. X.: Simulation of the effect of root distribution on hydraulic redistribution in a desert riparian forest, Ecological research, 28, 653-662, 2013b.
Hastings, W. K.: Monte Carlo sampling methods using Markov chains and their applications, 1970.
Hillel, D.: Introduction to environmental soil physics, Elsevier2003.
Hou, E., Litvak, M. E., Rudgers, J. A., Jiang, L., Collins, S. L., Pockman, W. T., Hui, D., Niu, S., and Luo, Y.: Divergent responses of primary production to increasing precipitation variability in global drylands, Glob Chang Biol, 27, 5225-5237, 10.1111/gcb.15801, 2021.
Howard, A. R., Van Iersel, M. W., Richards, J. H., and Donovan, L. A.: Night‐time transpiration can decrease hydraulic redistribution, Plant, Cell & Environment, 32, 1060-1070, 2009.
Hultine, K. R., Cable, W. L., Burgess, S. S. O., and Williams, D. G.: Hydraulic redistribution by deep roots of a Chihuahuan Desert phreatophyte, Tree Physiology, 23, 353-360, DOI 10.1093/treephys/23.5.353, 2003.
Jiang, J., Huang, Y., Ma, S., Stacy, M., Shi, Z., Ricciuto, D. M., Hanson, P. J., and Luo, Y.: Forecasting responses of a northern peatland carbon cycle to elevated CO2 and a gradient of experimental warming, Journal of Geophysical Research: Biogeosciences, 123, 1057-1071, 10.1002/2017jg004040, 2018.
Katul, G. G. and Siqueira, M. B.: Biotic and abiotic factors act in coordination to amplify hydraulic redistribution and lift, The New Phytologist, 187, 3-6, 2010.
Kohler, M. A. and Linsley, R. K.: Predicting the runoff from storm rainfall, US Department of Commerce, Weather Bureau1951.
Lee, E., Kumar, P., Barron-Gafford, G. A., Hendryx, S. M., Sanchez-Cañete, E. P., Minor, R. L., Colella, T., and Scott, R. L.: Impact of hydraulic redistribution on multispecies vegetation water use in a semiarid savanna ecosystem: An experimental and modeling synthesis, Water Resources Research, 54, 4009-4027, 10.1029/2017wr021006, 2018.
Li, X., Wei, Y., and Li, F.: Optimality of antecedent precipitation index and its application, Journal of Hydrology, 595, 126027, 2021.
Luo, Y. and Reynolds, J. F.: Validity of extrapolating field CO2 experiments to predict carbon sequestration in natural ecosystems, Ecology, 80, 1568-1583, 10.1890/0012-9658(1999)080[1568:Voefce]2.0.Co;2, 1999.
Luo, Y. and Schuur, E. A. G.: Model parameterization to represent processes at unresolved scales and changing properties of evolving systems, Glob Chang Biol, 26, 1109-1117, 10.1111/gcb.14939, 2020.
Marshall, L., Nott, D., and Sharma, A.: A comparative study of Markov chain Monte Carlo methods for conceptual rainfall‐runoff modeling, Water Resources Research, 40, 2004.

671 Meinzer, F. C., Brooks, J. R., Bucci, S., Goldstein, G., Scholz, F. G., and Warren, J. M.:
672 Converging patterns of uptake and hydraulic redistribution of soil water in contrasting
673 woody vegetation types, Tree Physiology, 24, 919-928, 10.1093/treephys/24.8.919, 2004.
674 Metropolis, N., Rosenbluth, A. W., Rosenbluth, M. N., Teller, A. H., and Teller, E.: Equation of
675 state calculations by fast computing machines, The journal of chemical physics, 21,
676 1087-1092, 1953.
677 Miele, F., Benettin, P., Wang, S., Retti, I., Asadollahi, M., Frutschi, M., Mohanty, B., Bernier‐
678 Latmani, R., and Rinaldo, A.: Spatially explicit linkages between redox potential cycles
679 and soil moisture fluctuations, Water Resources Research, 59, e2022WR032328, 2023.
680 Mosegaard, K. and Sambridge, M.: Monte Carlo analysis of inverse problems, Inverse problems,
681 18, R29, 2002.
682 Nadezhdina, N., Ferreira, M. I., Conceição, N., Pacheco, C. A., Häusler, M., and David, T. S.:
683 Water uptake and hydraulic redistribution under a seasonal climate: long‐term study in
684 a rainfed olive orchard, Ecohydrology, 8, 387-397, 2015.
685 Nadezhdina, N., David, T. S., David, J. S., Ferreira, M. I., Dohnal, M., Tesař, M., Gartner, K.,
686 Leitgeb, E., Nadezhdin, V., and Cermak, J.: Trees never rest: the multiple facets of
687 hydraulic redistribution, Ecohydrology, 3, 431-444, 2010.
688 Neumann, R. B. and Cardon, Z. G.: The magnitude of hydraulic redistribution by plant roots: a
689 review and synthesis of empirical and modeling studies, New Phytol, 194, 337-352,
690 10.1111/j.1469-8137.2012.04088.x, 2012.
691 Neumann, R. B., Cardon, Z. G., TESHERA‐LEVYE, J., Rockwell, F. E., Zwieniecki, M. A.,
692 and Holbrook, N. M.: Modelled hydraulic redistribution by sunflower (H elianthus
693 annuus L.) matches observed data only after including night‐time transpiration, Plant,
694 Cell & Environment, 37, 899-910, 2014.
695 Nicola, M. and Ram, O.: Rhizosphere water content drives hydraulic redistribution: Implications
696 of pore-scale heterogeneity to modeling diurnal transpiration in water-limited
697 ecosystems, Agricultural and Forest Meteorology, 312,
698 10.1016/j.agrformet.2021.108720, 2022.
699 Novick, K. A., Ficklin, D. L., Baldocchi, D., Davis, K. J., Ghezzehei, T. A., Konings, A. G.,
700 MacBean, N., Raoult, N., Scott, R. L., and Shi, Y.: Confronting the water potential
701 information gap, Nature Geosci, 15, 158-164, 2022.
702 Prăvălie, R.: Drylands extent and environmental issues. A global approach, Earth-Science
703 Reviews, 161, 259-278, 2016.
704 Prieto, I., Armas, C., and Pugnaire, F. I.: Water release through plant roots: new insights into its
705 consequences at the plant and ecosystem level, New Phytol, 193, 830-841,
706 10.1111/j.1469-8137.2011.04039.x, 2012.
707 Priyadarshini, K. V. R., Prins, H. H. T., de Bie, S., Heitkönig, I. M. A., Woodborne, S., Gort, G.,
708 Kirkman, K., Ludwig, F., Dawson, T. E., and de Kroon, H.: Seasonality of hydraulic
709 redistribution by trees to grasses and changes in their water‐source use that change
710 tree–grass interactions, Ecohydrology, 9, 218-228, 10.1002/eco.1624, 2016.
711 Quijano, J. C. and Kumar, P.: Numerical simulations of hydraulic redistribution across climates:
712 The role of the root hydraulic conductivities, Water Resources Research, 51, 8529-8550,
713 10.1002/2014wr016509, 2015.
714 Rawls, W. J., Brakensiek, D. L., and Saxtonn, K.: Estimation of soil water properties,
715 Transactions of the ASAE, 25, 1316-1320, 1982.

716 Romme, W. H., Allen, C. D., Bailey, J. D., Baker, W. L., Bestelmeyer, B. T., Brown, P. M.,
717 Eisenhart, K. S., Floyd, M. L., Huffman, D. W., and Jacobs, B. F.: Historical and modern
718 disturbance regimes, stand structures, and landscape dynamics in pinon–juniper
719 vegetation of the western United States, Rangeland Ecology & Management, 62, 203-
720 222, 2009.
721 Ryel, R., Caldwell, M., Yoder, C., Or, D., and Leffler, A.: Hydraulic redistribution in a stand of
722 Artemisia tridentata: evaluation of benefits to transpiration assessed with a simulation
723 model, Oecologia, 130, 173-184, 10.1007/s004420100794, 2002.
724 Saito, T., Fujimaki, H., Yasuda, H., and Inoue, M.: Empirical temperature calibration of
725 capacitance probes to measure soil water, Soil Science Society of America Journal, 73,
726 1931-1937, 2009.
727 Sardans, J. and Peñuelas, J.: Hydraulic redistribution by plants and nutrient stoichiometry: Shifts
728 under global change, Ecohydrology, 7, 1-20, 2014.
729 Schwinning, S., Litvak, M. E., Pockman, W. T., Pangle, R. E., Fox, A. M., Huang, C. W., and
730 McIntire, C. D.: A 3-dimensional model of Pinus edulis and Juniperus monosperma root
731 distributions in New Mexico: implications for soil water dynamics, Plant Soil, 450, 337-
732 355, 10.1007/s11104-020-04446-y, 2020.
733 Scott, R. L., Cable, W. L., and Hultine, K. R.: The ecohydrologic significance of hydraulic
734 redistribution in a semiarid savanna, Water Resources Research, 44,
735 10.1029/2007wr006149, 2008.
736 Seneviratne, S. I., Corti, T., Davin, E. L., Hirschi, M., Jaeger, E. B., Lehner, I., Orlowsky, B.,
737 and Teuling, A. J.: Investigating soil moisture–climate interactions in a changing climate:
738 A review, Earth-Science Reviews, 99, 125-161, 2010.
739 Tang, J., Riley, W. J., and Niu, J.: Incorporating root hydraulic redistribution in CLM 4.5:
740 Effects on predicted site and global evapotranspiration, soil moisture, and water storage,
741 Journal of Advances in Modeling Earth Systems, 7, 1828-1848, 2015.
742 Ukkola, A. M., De Kauwe, M. G., Roderick, M. L., Burrell, A., Lehmann, P., and Pitman, A. J.:
743 Annual precipitation explains variability in dryland vegetation greenness globally but not
744 locally, Global Change Biology, 27, 4367-4380, 2021.
745 Wei, L., Qiu, Z., Zhou, G., Zuecco, G., Liu, Y., and Wen, Y.: Soil water hydraulic redistribution
746 in a subtropical monsoon evergreen forest, Science of The Total Environment, 835,
747 155437, 10.1016/j.scitotenv.2022.155437, 2022.
748 Weng, E. and Luo, Y.: Soil hydrological properties regulate grassland ecosystem responses to
749 multifactor global change: A modeling analysis, Journal of Geophysical Research:
750 Biogeosciences, 113, 10.1029/2007jg000539, 2008.
751 Williams, M., Rastetter, E., Fernandes, D., Goulden, M., Wofsy, S., Shaver, G., Melillo, J.,
752 Munger, J., Fan, S. M., and Nadelhoffer, K.: Modelling the soil‐plant‐atmosphere
753 continuum in a Quercus–Acer stand at Harvard Forest: The regulation of stomatal
754 conductance by light, nitrogen and soil/plant hydraulic properties, Plant, Cell &
755 Environment, 19, 911-927, 1996.
756 Willmott, C. J. and Matsuura, K.: Advantages of the mean absolute error (MAE) over the root
757 mean square error (RMSE) in assessing average model performance, Climate research,
758 30, 79-82, 2005.
759 Wu, H., Fu, C., Wu, H., and Zhang, L.: Influence of the dry event induced hydraulic
760 redistribution on water and carbon cycles at five AsiaFlux forest sites: A site study

combining measurements and modeling, Journal of Hydrology, 587, 124979, 10.1016/j.jhydrol.2020.124979, 2020.
Xu, T., White, L., Hui, D., and Luo, Y.: Probabilistic inversion of a terrestrial ecosystem model: Analysis of uncertainty in parameter estimation and model prediction, Global Biogeochemical Cycles, 20, 10.1029/2005gb002468, 2006.
Yan, B. and Dickinson, R. E.: Modeling hydraulic redistribution and ecosystem response to droughts over the Amazon basin using Community Land Model 4.0 (CLM4), Journal of Geophysical Research: Biogeosciences, 119, 2130-2143, 10.1002/2014jg002694, 2014.
Yang, G., Huang, L., and Shi, Y.: Magnitude and determinants of plant root hydraulic redistribution: A global synthesis analysis, Frontiers in Plant Science, 13, 918585, 2022.
Yu, K. L. and D'Odorico, P.: Climate, vegetation, and soil controls on hydraulic redistribution in shallow tree roots, Advances in Water Resources, 66, 70-80, 10.1016/j.advwatres.2014.02.003, 2014.
Yu, T., Feng, Q., Si, J., Xi, H., Li, Z., and Chen, A.: Hydraulic redistribution of soil water by roots of two desert riparian phreatophytes in northwest China's extremely arid region, Plant Soil, 372, 297-308, 10.1007/s11104-013-1727-8, 2013.
Zhang, D., Madsen, H., Ridler, M. E., Kidmose, J., Jensen, K. H., and Refsgaard, J. C.: Multivariate hydrological data assimilation of soil moisture and groundwater head, Hydrology and Earth System Sciences, 20, 4341-4357, 2016.
Zheng, Z. and Wang, G.: Modeling the dynamic root water uptake and its hydrological impact at the Reserva Jaru site in Amazonia, Journal of Geophysical Research: Biogeosciences, 112, 2007.
Zhu, S., Chen, H., Zhang, X., Wei, N., Shangguan, W., Yuan, H., Zhang, S., Wang, L., Zhou, L., and Dai, Y.: Incorporating root hydraulic redistribution and compensatory water uptake in the Common Land Model: Effects on site level and global land modeling, Journal of Geophysical Research: Atmospheres, 122, 7308-7322, 2017.